Relevant Material for Lecture 9

"Galaxies: Structure, Dynamics, and Evolution"

5 Structure on larger scales

5.1 The content of massive halos: groups, clusters

Many halos contain more than one galaxy. Obvious examples are clusters - which can contain hundreds of galaxies. More mundane clusters are those with lower masses, and we call those groups. Most "normal" galaxies are member of a group. Take for example our Milky Way, which is part of the Local Group. This group contains 2 massive galaxies (MW, Andromeda), and several lower mass galaxies (Magellanic Clouds, M33, M32, NGC 205, ...), and many more lower mass galaxies. The local group is shown below:

Table 4.3 Local Group members

Name	Alternate Name	Coordinates RA (1950) Dec	Type	Distance (kpc)	M_V
M31	NGC 224	00 40.0 +40 59	Sb	725	−21.1
Milky Way	Galaxy	17 42.4 −28 55	Sbc	8	−20.6
M33	NGC 598	01 31.1 +30 24	Sc	795	−18.9
LMC		05 24.0 −69 48	Irr	49	−18.1
IC 10		00 17.7 +59 01	Irr	1250	−17.6
NGC 6822	DDO 209	19 42.1 −14 56	Irr	540	−16.4
M32	NGC 221	00 40.0 +40 36	dE2	725	−16.4
NGC 205		00 37.6 +41 25	dE5	725	−16.3
SMC		00 51.0 −73 06	Irr	58	−16.2
NGC 3109	DDO 236	10 00.8 −25 55	Irr	1260	−15.8
NGC 185		00 36.2 +48 04	dE3	620	−15.3
IC 1613	DDO 8	01 02.2 +01 51	Irr	765	−14.9
NGC 147	DDO 3	00 30.5 +48 14	dE4	589	−14.8
Sextans A	DDO 75	10 08.6 −04 28	Irr	1450	−14.4
Sextans B	DDO 70	09 57.4 +05 34	Irr	1300	−14.3
WLM	DDO 221	23 59.4 −15 45	Irr	940	−14.0
Sagittarius		18 51.9 −30 30	dSph/E7	24	−14.0
Fornax		02 37.8 −34 44	dSph/E3	131	−13.0
Pegasus	DDO 216	23 26.1 +14 28	Irr	759	−12.7
Leo I	DDO 74	10 05.8 +12 33	dSph/E3	270	−12.0
Leo A	DDO 69	09 56.5 +30 59	Irr	692	−11.7
And II		01 13.5 +33 09	dSph/E3	587	−11.7
And I		00 43.0 +37 44	dSph/E0	790	−11.7
SagDIG		19 27.9 −17 47	Irr	1150	−11.0
Antlia		10 01.8 −27 05	dSph/E3	1150	−10.7
Sculptor		00 57.6 −33 58	dSph/E3	78	−10.7
And III		00 32.6 +36 12	dSph/E6	790	−10.2
Leo II	DDO 93	11 10.8 +22 26	dSph/E0	230	−10.2
Sextans		10 10.6 −01 24	dSph/E4	90	−10.0
Phoenix		01 49.0 −44 42	Irr	390	− 9.9
LGS 3		01 01.2 +21 37	Irr	760	− 9.7
Tucana		22 38.5 −64 41	dSph/E5	900	− 9.6
Carina		06 40.4 −50 55	dSph/E4	87	− 9.2
Ursa Minor	DDO 199	15 08.2 +67 23	dSph/E5	69	− 8.9
Draco	DDO 208	17 19.2 +57 58	dSph/E3	76	− 8.6

SOURCE: From data kindly provided by M. Irwin.

The 3D distribution is

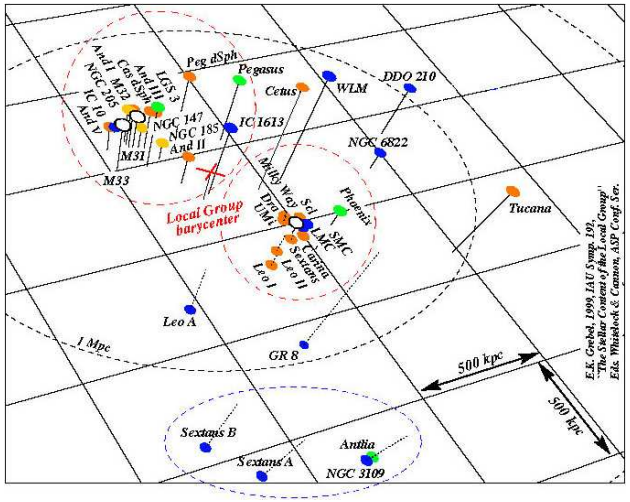

Some galaxies behind the plane of the Milky Way may still be missed. Studies of the Local Group are very useful: they give a indication of the full variation of galaxy properties as a function of luminosity and mass. Furthermore, individual stars can be detected in these system.
The local group is clearly not in equilibrium. At some stage, the MW and Andromeda will merge, and will form 1 big system. At that time, the two halos wil have merged too. Hence, at the moment the two galaxies are gravitationally bound, but have not yet collapsed yet.
The mass of the local group can be estimated from the so called timing argument. The MW and Andromeda approach each other with a velocity of about 120 km/s. Hence, whereas in the early days of the universe they were moving away from each other, their velocities have reversed, and they are now on a collision course.

This can only happen if they are massive enough - otherwise they would not be bound. One can estimate the total mass by requiring that they have a relative velocity of 120 km/s at an age of 14 Gyr, and a distance of 700 kpc. One finds that the mass should be $3\ 10^{12}\ M_{\odot}$. Much larger than the luminosity of $4\ 10^{10}\ L_{\odot}$. Hence the $M/L \approx 70 M_{\odot}/L_{\odot}$: there must be a lot of Dark Matter.

Other nearby groups

Well known other nearby groups are the Sculptor group, Maffei group, M81 group, Canes I group. See http://en.wikipedia.org/wiki/Virgo_ Supercluster

These have distances of $< 7Mpc$

Large nearby clusters are the Virgo clusters, and the Fornax cluster (at $\approx\ 1000km/s$, or 10-15 Mpc). A very massive nearby cluster is the Coma cluster (at 100 Mpc)

Groups and clusters are found from redshift catalogs, like the SDSS catalogue, or others. Usually one defines an algorithm like "a group is a system with an overdensity of X above the average".

One has to take special care about the fact that the dispersions in groups can be quite high (up to 1600 km/s in clusters). Hence the distance cannot be calculated straight from the Hubble Flow. In such cases, one has to search for overdensities in a velocity interval (say, of 500 or 1000 km/s), and in the 2 coordinates of the sky.

An additional complication is that some catalogues are incomplete. The SDSS spectroscopic sample is incomplete for galaxies with nearby neighbors. This is due to the fact that the fibers cannot be close together. This makes it harder to define groups, and careful corrections are needed for the catalogues.

This probably makes it clear that the definition of groups and clusters is never easy from observational material. This has never stopped anybody from making such catalogues.

Once a catalogue of groups/clusters has been built, one can construct the "mass function", the number density as a function of mass. Below is an example from Heinamaki et al (A&A 397, 63)

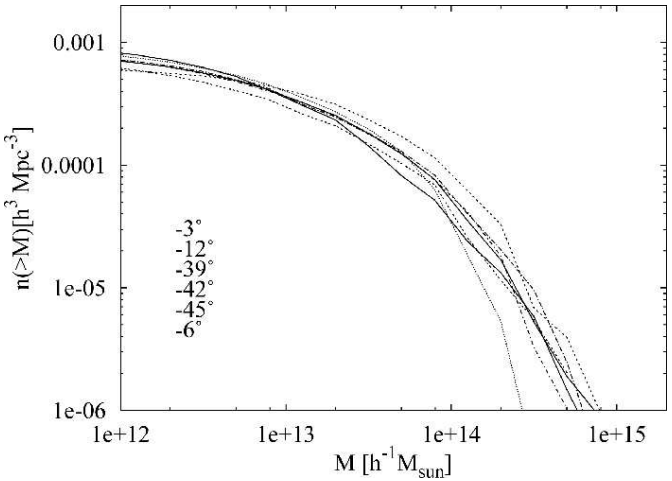

This graph shows the cumulative density ($n(> M)$, the number density of groups larger than M), as a function of M. It is clear that groups have very large masses, from 10^{12} to 10^{15} Notice that clusters like the Coma cluster (with $M \approx 10^{15} M_{\odot}$ are rare (10^{-6} Mpc^{-3}), or $\approx$ 1 every 100 Mpc.

The velocity dispersions correlate well with mass as shown by the same authors:

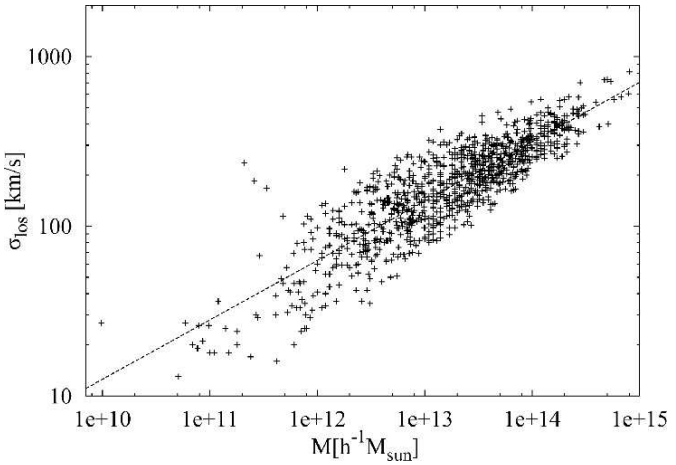

Groups and clusters are the largest collapsed systems, but structure on larger scales exist. This is measured statistically. We express this by the correlation function. The correlation function describes how the probability of finding another galaxy in the neighborhood of a galaxy increases with decreasing distance.

7.3.1 Correlation Functions

Galaxies are not randomly distributed in space, but rather they gather in groups, clusters, or even larger structures. Phrased differently, this means that the probability of finding a galaxy at location $\boldsymbol{x}$ is not independent of whether there is a galaxy in the vicinity of $\boldsymbol{x}$. It is more probable to find a galaxy in the vicinity of another one than at an arbitrary location. This phenomenon is described such that one considers two points $\boldsymbol{x}$ and $\boldsymbol{y}$, and two volume elements $\mathrm{d}V$ around these points. If $\overline{n}$ is the average number density of galaxies, the probability of finding a galaxy in the volume element $\mathrm{d}V$ around $\boldsymbol{x}$ is then

$$P_1 = \overline{n}\,\mathrm{d}V\,,$$

independent of $\boldsymbol{x}$ if we assume that the Universe is statistically homogeneous. We choose $\mathrm{d}V$ such that $P_1 \ll 1$, so that the probability of finding two or more galaxies in this volume element is negligible.

The probability of finding a galaxy in the volume element $\mathrm{d}V$ at location $\boldsymbol{x}$ and at the same time finding a galaxy in the volume element $\mathrm{d}V$ at location $\boldsymbol{y}$ is then

$$P_2 = (\overline{n}\,\mathrm{d}V)^2\left[1+\xi_{\mathrm{g}}(\boldsymbol{x},\boldsymbol{y})\right]\,. \tag{7.17}$$

If the distribution of galaxies was uncorrelated, the probability P_2 would simply be the product of the probabilities of finding a galaxy at each of the locations $\boldsymbol{x}$ and $\boldsymbol{y}$ in a volume element $\mathrm{d}V$, so $P_2 = P_1^2$. But since the distribution is correlated, the relation does not apply in this simple form; rather, it needs to be modified, as was done in (7.17). Equation (7.17) defines the *two-point correlation function* (or simply "correlation function") of galaxies $\xi_{\mathrm{g}}(\boldsymbol{x},\boldsymbol{y})$.

By analogy to this, the correlation function for the total matter density can be defined as

$$\begin{aligned}\langle\rho(\boldsymbol{x})\,\rho(\boldsymbol{y})\rangle &= \overline{\rho}^2\,\langle[1+\delta(\boldsymbol{x})]\,[1+\delta(\boldsymbol{y})]\rangle \\ &= \overline{\rho}^2\,(1+\langle\delta(\boldsymbol{x})\,\delta(\boldsymbol{y})\rangle) \\ &=: \overline{\rho}^2\,[1+\xi(\boldsymbol{x},\boldsymbol{y})]\,,\end{aligned} \tag{7.18}$$

because the mean (or expectation) value $\langle\delta(\boldsymbol{x})\rangle = 0$ for all locations $\boldsymbol{x}$.

In the above equations, angular brackets denote averaging over an ensemble of distributions that all have identical statistical properties. In our example of the lake, the correlation function of the wave amplitudes at positions $\boldsymbol{x}$ and $\boldsymbol{y}$, for instance, would be determined by taking a large number of snapshots of its surface and then averaging the product of the amplitudes at these two locations over all these realizations.

Since the Universe is considered statistically homogeneous, ξ can only depend on the difference $\boldsymbol{x}-\boldsymbol{y}$ and not on $\boldsymbol{x}$ and $\boldsymbol{y}$ individually. Furthermore, ξ can only depend on the separation $r = |\boldsymbol{x}-\boldsymbol{y}|$, and not on the direction of the separation vector $\boldsymbol{x}-\boldsymbol{y}$ because of the assumed statistical isotropy of the Universe. Therefore, $\xi = \xi(r)$ is simply a function of the separation between two points.

For a homogeneous random field, the ensemble average can be replaced by spatial averaging, i.e., the correlation function can be determined by averaging over the density products for a large number of pairs of points with given separation r. The equivalence of ensemble average and spatial average is called the ergodicity of the random field. Only by this can the correlation function (and all other statistical properties) in our Universe be measured at all, because we are able to observe only a single – namely our – realization of the hypothetical ensemble. From the measured correlations between galaxy positions, as determined from spectroscopic redshift surveys of galaxies (see Sect. 8.1.2), one finds the approximate relation

$$\xi_{\mathrm{g}}(r) = \left(\frac{r}{r_0}\right)^{-\gamma}\,, \tag{7.19}$$

for galaxies of luminosity $\sim L^*$ (see Fig. 7.4), where $r_0 \simeq 5h^{-1}\,\mathrm{Mpc}$ denotes the correlation length, and

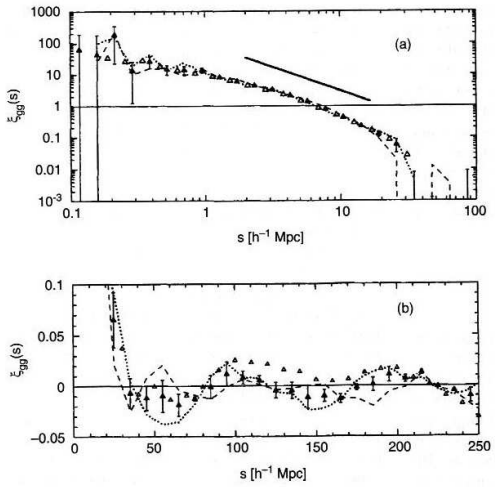

Fig. 7.4. The correlation function ξ_{g} of galaxies, as it was determined from the Las Campanas Redshift Survey. In the top panel, ξ_{g} is shown for small and intermediate separations, whereas the bottom panel shows it for large separations. Dashed and dotted lines indicate the northern and southern part, respectively, of the survey, and the solid triangles denote the correlation function obtained from combining both. A power law with slope $\gamma = 1.52$ is plotted for comparison (bold solid curve)

where the slope is about $\gamma \simeq 1.8$. This relation is approximately valid over a range of separations $2h^{-1}\,\mathrm{Mpc} \lesssim r \lesssim 30h^{-1}\,\mathrm{Mpc}$.

Hence, the correlation function provides a means to characterize the structure of the matter distribution in the Universe. Besides this two-point correlation function, correlations of higher order may also be defined, leading to general n-point correlation functions. These are more difficult to determine from observation, though. It can be shown that the statistical properties of a random field are fully specified by the set of all n-point correlations.

7.3.2 The Power Spectrum

An alternative (and equivalent) description of the statistical properties of a random field, and thus of the structure of the Universe, is the *power spectrum* $P(k)$. Roughly speaking, the power spectrum $P(k)$ describes the level of structure as a function of the length-scale $L \simeq 2\pi/k$; the larger $P(k)$, the larger the amplitude of the fluctuations on a length-scale $2\pi/k$. Here, k is a *wave number*. Phrased differently, the density fluctuations are decomposed into a sum of plane waves of the form $\delta(\boldsymbol{x}) = \sum a_{\boldsymbol{k}}\,\cos(\boldsymbol{x}\cdot\boldsymbol{k})$, with a wave vector $\boldsymbol{k}$ and an amplitude $a_{\boldsymbol{k}}$. The power spectrum $P(k)$ then describes the distribution of amplitudes with equal $k = |\boldsymbol{k}|$. Technically speaking, this is a Fourier decomposition. Referring back to the example of waves on the surface of a lake, one finds that a characteristic wavelength L_{c} exists, which depends, among other factors, on the wind speed. In this case, the power spectrum will have a prominent maximum at $k = 2\pi/L_{\mathrm{c}}$.

The power spectrum $P(k)$ and the correlation function are related through a Fourier transform; formally, one has[3]

$$P(k) = 2\pi\int_0^\infty \mathrm{d}r\,r^2\,\frac{\sin kr}{kr}\,\xi(r)\,, \tag{7.20}$$

[3] This may not look like a "standard" Fourier transform on first sight. However, the relation between $P(k)$ and $\xi(r)$ is given by a three-dimensional Fourier transform. Since the correlation function depends only on the separation $r = |\boldsymbol{r}|$, the two integrals over the angular coordinates can be performed explicitly, leading to the form of (7.20).

i.e., the integral over the correlation function with a weight factor depending on $k \sim 2\pi/L$. This relation can also be inverted, and thus $\xi(r)$ can be computed from $P(k)$.

In general, knowing the power spectrum is not sufficient to unambiguously describe the statistical properties of any random field – in the same way as the correlation function $\xi(r)$ only provides an incomplete characterization. However, random fields do exist, so-called *Gaussian random fields*, which are uniquely characterized by $P(k)$. Such Gaussian random fields play an important role in cosmology because it is assumed that at very early epochs, the density field obeyed Gaussian statistics.

7.4 Evolution of Density Fluctuations

$P(k)$ and $\xi(r)$ both depend on cosmological time or redshift because the density field in the Universe evolves over time. Therefore, the dependence on t is explicitly written $P(k, t)$ and $\xi(r, t)$. Note that $P(k, t)$ is linearly related to $\xi(r, t)$, according to (7.20), and ξ in turn depends quadratically on the density contrast δ. If we interpret $\boldsymbol{x}$ as a *comoving* separation vector, from (7.14) we then know the time dependence of the density fluctuations, $\delta(\boldsymbol{x}, t) = D_+(t)\delta_0(\boldsymbol{x})$. Thus, within the scope of the validity of (7.14),

$$\xi(x, t) = D_+^2(t)\,\xi(x, t_0)\,, \tag{7.21}$$

and accordingly

$$P(k, t) = D_+^2(t)\,P(k, t_0) =: D_+^2(t)\,P_0(k)\,, \tag{7.22}$$

where k is a *comoving wave number*. We shall stress once again that these relations are valid only in the framework of Newtonian, linear perturbation theory in the matter dominated era of the Universe, to which we had restricted ourselves in Sect. 7.2.2. Equation (7.22) states that the knowledge of $P_0(k)$ is sufficient to obtain the power spectrum $P(k, t)$ at any time, again within the framework of linear perturbation theory.

7.4.1 The Initial Power Spectrum

The Harrison–Zeldovich Spectrum. Initially it may seem as if $P_0(k)$ is a function that can be chosen arbitrarily, but one objective of cosmology is to calculate this power spectrum and to compare it to observations. More than thirty years ago, arguments were already developed to specify the functional form of the initial power spectrum.

At early times, the expansion of the Universe follows a power law, $a(t) \propto t^{1/2}$ in the radiation-dominated era. At that time, no natural length-scale existed in the Universe to which one might compare a wavelength. The only mathematical function that depends on a length but does not contain any characteristic scale is a power law;[4] hence for very early times one should expect

$$P(k) \propto k^{n_s}\,. \tag{7.23}$$

Many years ago, Harrison, Zeldovich, Peebles and others argued, based on scaling relations, that it should be $n_s = 1$. For this reason, the spectrum (7.23) with $n_s = 1$ is called *Harrison–Zeldovich spectrum*. With such a spectrum, we may choose a time t_i after the inflationary epoch and write

$$P(k, t_i) = D_+^2(t_i)\,A\,k^{n_s}\,, \tag{7.24}$$

where A is a normalization constant that cannot be determined from theory but has to be fixed by observations. Assuming the validity of (7.22),

$$P_0(k) = A\,k^{n_s}$$

would then apply.

The Transfer Function. This relation above needs to be modified for several reasons. In linear perturbation theory, which led to $\delta(\boldsymbol{x}, t) = D_+(t)\,\delta_0(\boldsymbol{x})$, we assumed the validity of Newtonian dynamics, considered only the matter-dominated epoch of the Universe, and disregarded any pressure terms. The evolution of perturbations in the radiation-dominated cosmos proceeds differently though, also depending on the scale of the perturbations in comparison to the length of the horizon, so that a correction term of the form

$$P_0(k) = A\,k^{n_s}\,T^2(k) \tag{7.25}$$

[4] You can convince yourself of this by trying to find another type of function of a scale that does not involve a characteristic length; e.g., $\sin x$ does not work if x is a length, since the sine of a length is not defined; one thus needs something like $\sin(x/x_0)$, hence introducing a length-scale. The same arguments apply to other functions, such as the logarithm, the exponential, etc. Also note that the sum of two power laws, e.g., $Ax^\alpha + Bx^\beta$ defines a characteristic scale, namely that value of x where the two terms become equal.

Interpretation of clustering

The clustering of galaxies out to 10Mpc or more shows that galaxies are correlated on very large scales. How come ? It is not due to clusters - clusters are too rare to produce this effect.
It is also not due to groups - they are generally much smaller - they play a role below 1 Mpc.
The cause for the clustering signal is therefore truely due to the fact that it is more likely to have a neighboring galaxy which is unbound. It can be seen "by eye" in redshift slices:

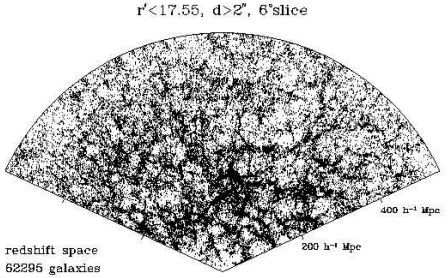

The galaxy distribution shows obviously structure out to very large scales (up to 30Mpc). Hence the powerspectrum will be non-zero out to 30Mpc - and the correlation function too.

5.3 Origin of clustering

One may wonder how it is possible that the galaxies are clustered at such large distances. The main reason is due to the clustering of halos. It is directly related to the formation of galaxies:
Halos (and galaxies inside them) form from small per-

turbations in the early universe which grow with time. The halos which have formed, are those halos which had time to collapse. In general, small perturbations form before large perturbations. Theory predicts that the perturbations have a powerspectrum which looks like this

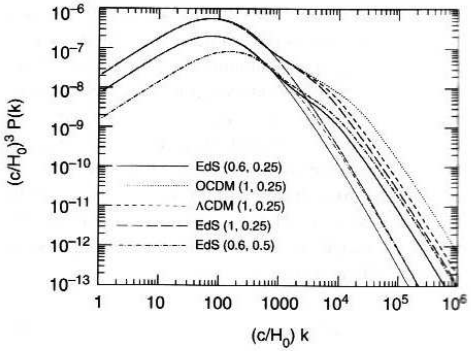

Fig. 7.6. The current power spectrum of density fluctuations for CDM models. The wave number k is given in units of H_0/c. and $(H_0/c)^3\,P(k)$ is dimensionless. The various curves have different cosmological parameters: EdS: $\Omega_m = 1$, $\Omega_\Lambda = 0$; OCDM: $\Omega_m = 0.3$, $\Omega_\Lambda = 0$; ΛCDM: $\Omega_m = 0.3$, $\Omega_\Lambda = 0.7$. The values in parentheses specify (σ_8, Γ), where σ_8 is the normalization of the power spectrum (which will be discussed below), and where Γ is the shape parameter. The thin curves correspond to the power spectrum $P_0(k)$ linearly extrapolated to the present day, and the bold curves take the non-linear evolution into account

The observed powerspectrum looks like this (Percival et al., astroph-0608636)

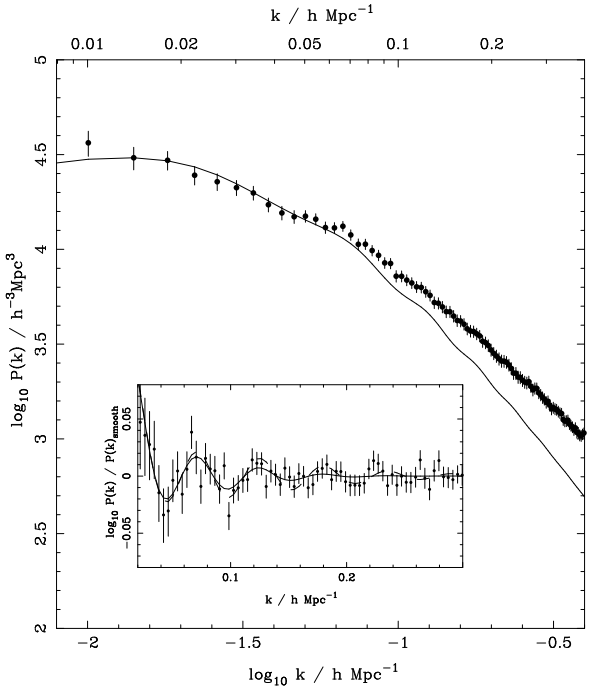

FIG. 12.— The redshift-space power spectrum recovered from the combined SDSS main galaxy and LRG sample, optimally weighted for both density changes and luminosity dependent bias (solid circles with 1-σ errors). A flat Λ cosmological distance model was assumed with $\Omega_M = 0.24$. Error bars are derived from the diagonal elements of the covariance matrix calculated from 2000 log-normal catalogues created for this cosmological distance model, but with a power spectrum amplitude and shape matched to that observed (see text for details). The data are correlated, and the width of the correlations is presented in Fig. 10 (the correlation between data points drops to < 0.33 for $\Delta k > 0.01\,h\,\mathrm{Mpc}^{-1}$). The correlations are smaller than the oscillatory features observed in the recovered power spectrum. For comparison we plot the model power spectrum (solid line) calculated using the fitting formulae of Eisenstein & Hu (1998); Eisenstein et al. (2005), for the best fit parameters calculated by fitting the WMAP 3-year temperature and polarisation data, $h = 0.73$, $\Omega_M = 0.24$, $n_s = 0.96$ and $\Omega_b/\Omega_M = 0.174$ (Spergel et al. 2006). The model power spectrum has been convolved with the appropriate window function to match the measured data, and the normalisation has been matched to that of the large-scale ($0.01 < k < 0.06\,h\mathrm{Mpc}^{-1}$) data. The deviation from this low Ω_M linear power spectrum is clearly visible at $k \gtrsim 0.06\,h\,\mathrm{Mpc}^{-1}$, and will be discussed further in Section 6. The solid circles with 1σ errors in the inset show the power spectrum ratioed to a smooth model (calculated using a cubic spline fit as described in Percival et al. 2006) compared to the baryon oscillations in the (WMAP 3-year parameter) model (solid line), and shows good agreement. The calculation of the matter density from these oscillations will be considered in a separate paper (Percival et al. 2006). The dashed line shows the same model without the correction for the damping effect of small-scale structure growth of Eisenstein et al. (2006). It is worth noting that this model is not a fit to the data, but a prediction from the CMB experiment.

The models are in general a very good fit to the data. Hence the correlation of galaxies is due to the correlation of halos, which is due to the same perturbations in the universe which caused the formation of galaxies.

We have seen earlier that perturbations grow in time. In the future, some of the large scale structure which we see now will lead to collapsed halos. In the same way, the rich clusters which we see now, did not exist at high redshift. At that time, they were "large scale structure".

We can now see why the correlation function is so important to measure: it relates directly to the perturbations in the early universe which formed galaxies.

There are a couple of important points:

- 1. The perturbations cause a powerspectrum of fluctuations for the full density distribution of matter $\rho(x)$. The distribution of the halos does not exactly follow $\rho(x)$. Halos have only formed in areas where the universe had time to collapse. Hence the clustering of halos is similar, but not identical to the clustering of matter.

- 2. Halo clustering depends on mass ! High mass halos are clustered more than low mass halos. The reason is the following: high mass halos are rare, and only arise in regions where there is a lot of excess material. These regions are those regions with strong, positive perturbations on even larger scales (see the figure below). These perturbations "push" the halos (which are smaller) over critical, and cause them to collapse. However, since they are large scale, they'll cause an excess of these halos in the general neighborhood - and hence these systems are strongly clustered.
  Low mass halos don't need these larger scale perturbations to form, and hence how lower clustering.

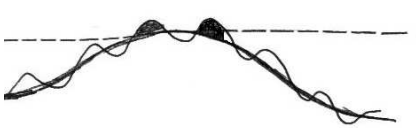

Clustering of massive halos: massive halos have to form from weak perturbations. They can only form when there are perturbations present on even larger scales (thick curve). This large-scale perturbation pushes several of the small scale perturbations over the limit (dashed horizontal line) so that they can collapse and form a halo. One expects to have these halos to have nearby neighbors near the peak of the large scale fluctuation. Hence the halos are more strongly clustered than the dark matter itself.

The figure below shows the results from a simulation (Mo & White 1996, MNRAS 282, 347

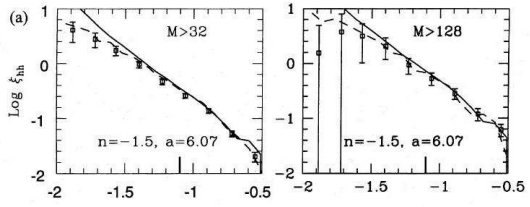

Correlation functions of clusters, in a simulation
As can be seen, the low mass clusters (left panel) are less strongly clustered than the high mass clusters.

6 Studying galaxy evolution - evolution of stellar populations

The formation of a galaxy can be traced back in time the easiest by determination of the ages of the stars. From that, we can derive the number of stars formed in at a time t, $t + dt$: $sfr(t)dt$. The function $sfr(t)$ is the star formation rate, and measuring this is a great way to characterize the formation history.

In practice, this is difficult. Unlike for nearby stars, we cannot take detailed spectra to measure age, and metallicity of the stars in external galaxies. Hence we have to resort to tricks.

Trick 1: Age determination for clusters

When we analyze clusters, we have a set of stars at the same distance, with the same age and metallicity. This makes the analysis much easier.

An observed color magnitude diagram looks like this

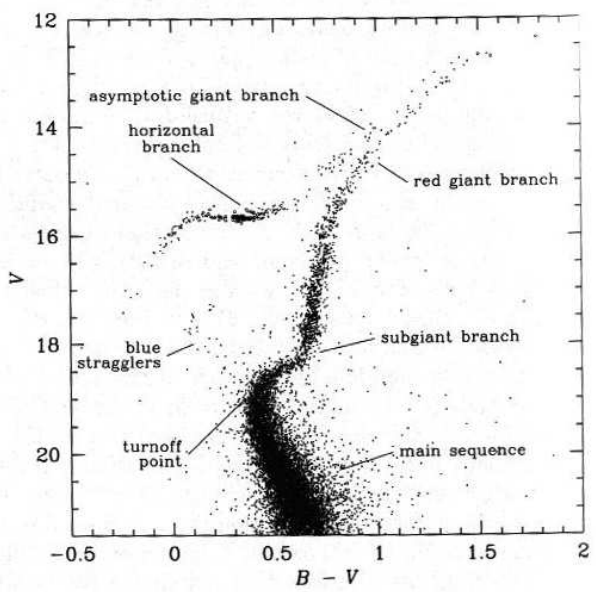

Figure 6.2 The color-magnitude diagram for the globular cluster M3. Known variable stars are shown as open circles, and the principal sequences are annotated. [From data published in Buonanno *et al.* (1994)]

Modeling these color magnitude diagrams works in the following way: Calculate the evolution of magnitude and color for a range of stellar populations, each with separate metallicity. For each population, calculate the evolution of stars with a range in masses. Then, connect the derived magnitudes and colors at a given age, at a range of masses, to show the "theoretical" color magnitude diagram. There are several tricky aspects, including the calculation of the detailed spectra of the stellar atmospheres, including all the metal-lines. Below is an example of theoretical color-magnitude

diagrams, for a range of ages:

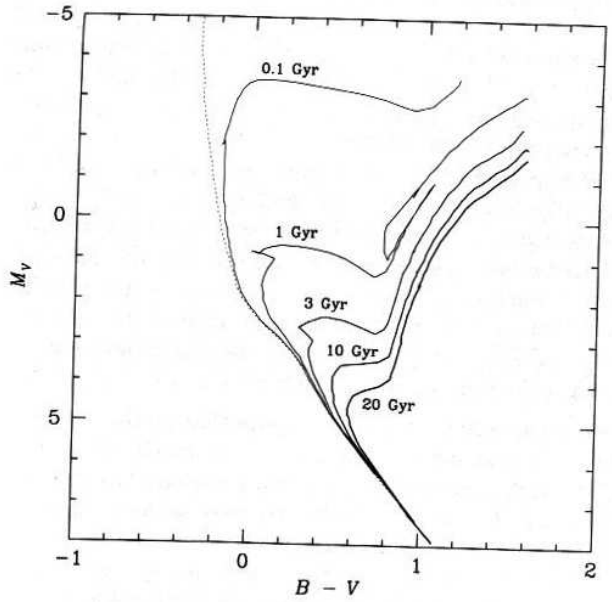

Figure 6.6 Theoretically calculated isochrones showing how a stellar population with $Z = 0.004$, $Y = 0.24$ evolves away from the ZAMS (dotted line) in the CM diagram. Each isochrones is labeled by its age. [From the calculations of Bertelli *et al.* (1994)]

It is clear from this that ages of clusters (open or globular) can be determined with a fairly good accuracy.

Applications

Dwarf galaxies close to the MW are very suitable, as it is straightforward to measure CMD to the main sequence. Some examples

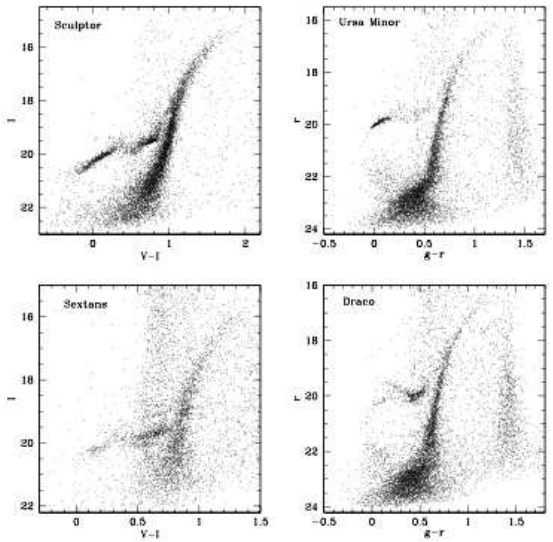

Figure 1. Wide Field CMDs of Sculptor, Ursa Minor, Draco & Sextans, taken with the INT/WFC and the ESO2.2m/WFI covering 30′ field of view for each galaxy (Letarte, Irwin & Tolstoy 2003, in prep.). These are all old galaxies, but their CMDs look different in several crucial respects.

These galaxies are old, and fairly simple.

Much more complex is the :

Carina dwarf galaxy

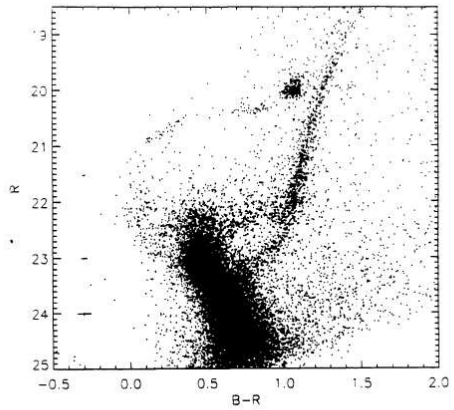

Figure 1. The CMD of the Carina dSph. The median internal photometric error at magnitudes $R = 21.5$, 23, and 24 are shown as on the left-hand side.

Compare this to:

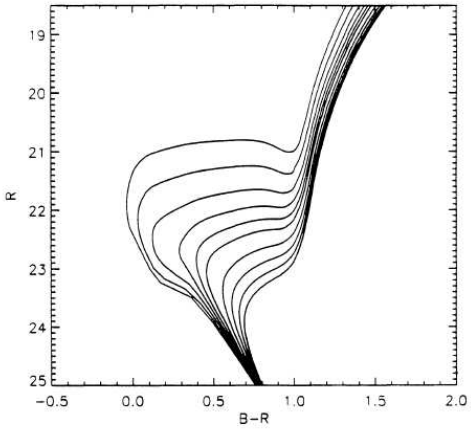

Figure 2. New theoretical isochrones from VandenBerg *et al.* (1996) for [Fe/H]= −1.84 and ages of 1.3, 2, 3, 4, 5, 6, 8, 10, 12, and 14 Gyr at the distance and reddening of the Carina dSph.

The galaxy obviously has had at least 3 bursts of star formation. This is a possible distribution of ages

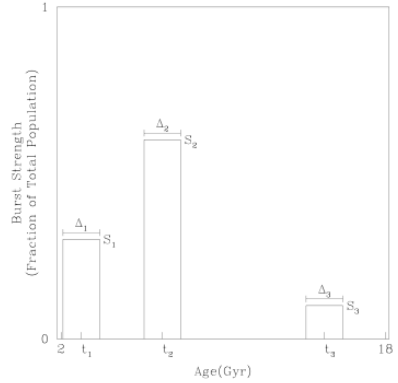

FIG. 13.—Parameterization of Carina's star formation history. We assumed three major episodes of star formation: t_i is the age of the episode in Gyr, Δ_i is the duration of the episode in Gyr, and S_i is the strength of the episode in a fraction of the total population. For reasons explained in the text, t_1, t_3, and Δ_3 are fixed at 3, 15, and 1 Gyr, respectively.

Going further, life gets tougher. The Magellanic clouds are still possible using HST. Some results are below:

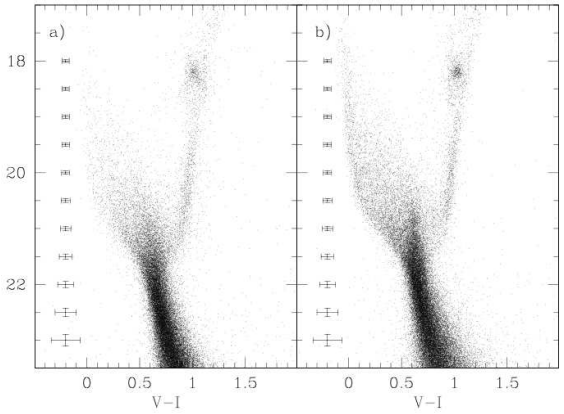

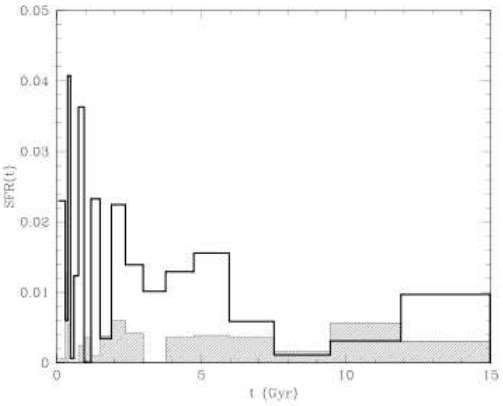

FIG. 5.—SFHs derived from the main-sequence LFs. *Thick line*: SFH bar; *shaded line*: 10 × SFH Disk 1. Units are $M_\odot$ yr^{-1} square degrees; the errors in each age bin are ≈ ±15%.

Going out even further, it is possible to use the RGB as an indicator - but the further one goes, the harder it gets to use individual stars.
For galaxies at Virgo distance, it is simply impossible to do any of this. In those cases, we have to rely on integrated properties of galaxies (colors, spectra).

Interpreting integrated properties of galaxies

Lacking the information about individual stars, we can still examine the integrated properties of galaxies. Obviously, a lot of information is lost. However, it is easy to imagine that we can just add up all the light from the stars to see how the total colors, and spectrum, vary with time.

There is at least one additional complication: the light from very luminous, but short phases can become relevant. Of special importance is the light from AGB stars. These stars are only short-lived, but very luminous. In normal CMDs, they are rare, and hence don't need to play a big role. But in integrated light they can be quite important. The same for HB stars, etc.
In short: there can be significant uncertainties.

input parameters

Before models can be made, the following input parameters have to be set

- Initial Mass Function $\phi(m)$. The distribution of stellar masses of a zero age stellar population. The number of stars between mass m and $m+dm$ is $\phi(m)$. It is often approximated by a Salpeter IMF $\phi(m) \propto m^{-2.35}$. However, it has become

clear that the Salpeter IMF overestimates the number of low mass stars. A Chabrier IMF or Kroupa IMF look similar to a Salpeter IMF at high masses, but has fewer low mass stars. The Chabrier IMF is given by:

$$m\phi(m) = exp\left[-\frac{(\log(m) - log(m_c))^2}{2\sigma^2}\right] \text{for m} \leq 1\ M_\odot$$

$$= m^{-1.3} \text{for m} \geq 1 M_\odot$$

with $m_c = 0.08 M_\odot$ and $\sigma = 0.69$

- Metallicity, and abundance ratios. The stellar evolution depends on metallicity. Furthermore, the spectra and the colors are influenced, and the line-blanketing by iron and other lines change the emitted light, as a function of metallicity (for a "constant" bolometric luminosity, temperature, size star). In general, evolution appears to slow down with higher metallicity: a star with higher metallicity evolves slower.

- Detailed models for stellar evolution. Various (subtle) differences exist between various models, even for "standard" phases like RGB. The modeling of rarer phases like AGB, HB, etc is even more uncertain at the moment.

- Spectra of stars with a given effective temperature, gravity, and metallicity. These are needed to convert the effective temperature and gravity of the model stars into observed spectra/colors. The spectra can be either empirical, or theoretical. Both have advantages and drawbacks. Empirical spectra will not cover all possible phases, and will have limited wavelength coverage. Theoretical spectra are often still wrong in a significant way.

- Star formation history. The simplest model is a SSP "single burst stellar population". However, nobody believes that galaxies form in a single burst. Hence we have to assume some kind of star formation history. This is usually either a constant star formation rate, or exponentially declining $sfr \propto exp(-t/\tau)$.

Results

The results by Bruzual & Charlot (2003) are used a lot (2003, MNRAS 344, 1000, BC03). It is an improvement on earlier models (BC93, BC96) Some characteristic results:

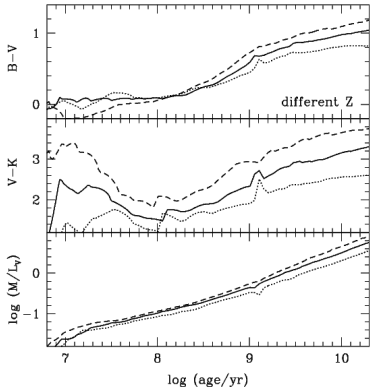

Figure 1. Evolution of the $B-V$ and $V-K$ colours and stellar mass-to-light ratio M/L_V of simple stellar populations for different metallicities, $Z = 0.004$ (dotted line), $Z = Z_\odot = 0.02$ (solid line) and $Z = 0.05$ (dashed line), for the standard model of Section 3. All models have the Chabrier (2003b) IMF truncated at 0.1 and 100 $M_\odot$ (see equation 2).

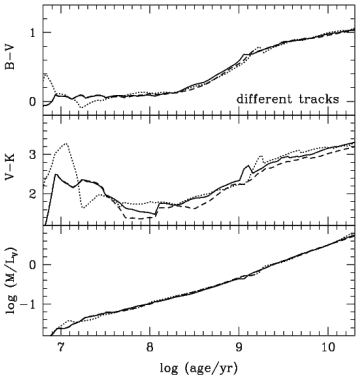

Figure 2. Evolution of the $B-V$ and $V-K$ colours and stellar mass-to-light ratio M/L_V of simple stellar populations of solar metallicity computed using the Geneva (dotted line), Padova 1994 (standard model; solid line) and Padova 2000 (dashed line) stellar evolution prescriptions and the STELIB/BaSeL 3.1 spectral calibration. All models have the Chabrier (2003b) IMF truncated at 0.1 and 100 $M_\odot$ (see equation 2).

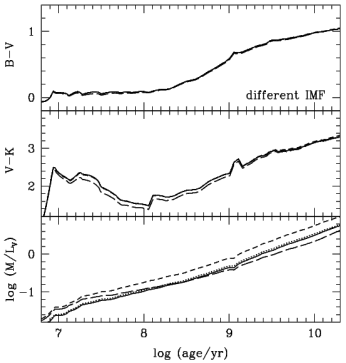

Figure 4. Evolution of the $B-V$ and $V-K$ colours and stellar mass-to-light ratio M/L_V of simple stellar populations of solar metallicity computed using the Padova 1994 stellar evolution prescription and the STELIB/BaSeL 3.1 spectral calibration, for different IMFs: Chabrier (2003b, standard model; solid line; see equation 2), Kroupa (2001, dotted line), Salpeter (1955, short-dashed line) and Scalo (1998, long-dashed line). All IMFs are truncated at 0.1 and 100 $M_\odot$.

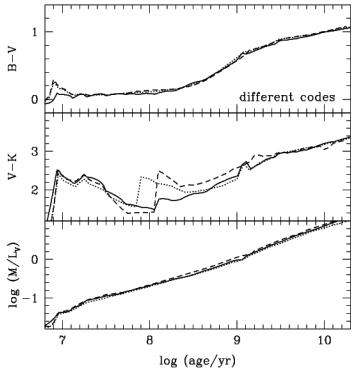

Figure 5. Evolution of the $B-V$ and $V-K$ colours and stellar mass-to-light ratio M/L_V of simple stellar populations of solar metallicity computed using our model (with the Padova 1994 stellar evolution prescription and the STELIB/BaSeL 2.2 spectral calibration; solid line), the Fioc & Rocca-Volmerange (1997) PÉGASE version 2.0 model (dotted line) and the Girardi et al. (2002) model (dashed line). All models have the Kroupa (2001) present-day IMF truncated at 0.01 and 100 $M_\odot$.

The PÉGASE model shows good general agreement with our model in Fig. 5. There are marked discrepancies at ages around 10^7 yr, where the PÉGASE model is redder in $B-V$ but bluer in $V-K$ than our model, and at ages around 10^8 yr, where it is nearly a magnitude redder in $V-K$. General agreement is expected because the PÉGASE model relies on the same Padova 1994 tracks as used in our model to describe the evolution of stars up to the end of the early-AGB and on the same BaSeL 2.2 spectral calibration. The discrepancy at early ages arises from a difference in the spectral calibration of stars hotter than 50 000 K. In the PÉGASE model, the spectra of these stars are taken from Clegg & Middlemass (1987), while in our model, they are taken from the more recent computations of Rauch (2002). The discrepancy in the $V-K$ colour at ages around 10^8 yr arises from a different prescription for TP-AGB evolution. Fioc & Rocca-Volmerange (1997) use 'typical' TP-AGB luminosities and evolutionary time-scales from Groenewegen & de Jong (1993),

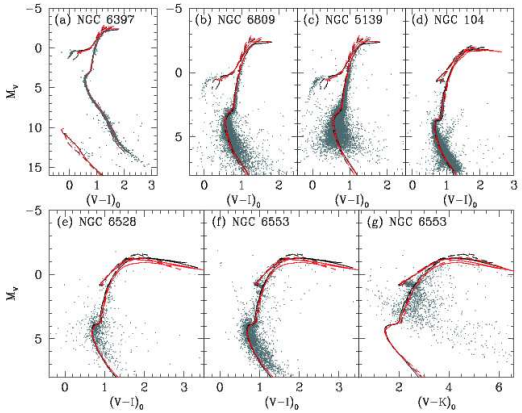

Figure 7. Comparison of model isochrones with observed colour–magnitude diagrams of six old Galactic globular clusters. For each cluster, the adopted distance modulus and colour excess are listed in Table 4 along with the sources of the stellar photometry. Each panel contains four isochrones: the red isochrones are computed using the Padova 1994 tracks, while the black isochrones are computed using the Padova 2000 tracks. In each case, the dashed and solid isochrones are computed using the BaSeL 1.0 and BaSeL 3.1 spectral calibrations, respectively. All isochrones pertaining to a given cluster have a fixed age and metallicity (see Table 4).

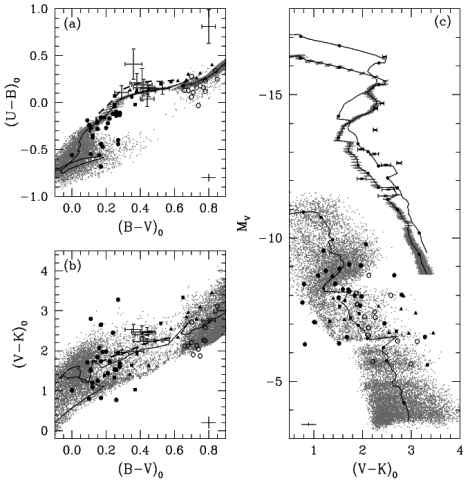

Figure 8. (a) $U-B$ versus $B-V$ and (b) $V-K$ versus $B-V$ integrated colours of star clusters. The different symbols represent LMC globular clusters in various age ranges according to the SWB classification scheme (classes I–III, filled circles; class IV, squares; class V, triangles; classes VI–VII, open circles). The $U-B$ and $B-V$ colours are from van den Bergh (1981) and the $V-K$ colours from Persson et al. (1983). The points with error bars are young star clusters in the merger remnant galaxy NGC 7252 (Miller et al. 1997; Maraston et al. 2001). The solid line shows the evolution of the standard SSP model of Section 3 for the metallicity $Z = 0.4\,Z_\odot$ at ages from a few Myr to 13 Gyr. The small dots show the results of 22 000 stochastic realizations of the integrated colours of clusters of mass $2 \times 10^4\,M_\odot$ at ages between 10^5 yr and 13 Gyr, for the same metallicity and IMF as for this SSP model. The heavy dashed line shows the colours of the standard SSP model of Section 3 for the metallicity $Z = Z_\odot$ at ages from 100 Myr to 1 Gyr. (c) Absolute magnitude M_V versus $V-K$ colour. The data are the same as in (a) and (b). Three models show the evolution of, from bottom to top, a $2 \times 10^4\,M_\odot$ SSP with metallicity $Z = 0.4\,Z_\odot$, a $3 \times 10^6\,M_\odot$ SSP with metallicity $Z = Z_\odot$ and a $6 \times 10^6\,M_\odot$ SSP with metallicity $Z = Z_\odot$. Small circles indicate the positions of the models at the ages 6, 7, 10, 100, 400 and 500 Myr and 1, 1.4, 2 and 10 Gyr (these marks can be used to roughly date the clusters). Stochastic realizations of integrated colours are shown only for the two least massive models, as the predicted scatter is small for the most massive one. Typical observational error bars are indicated at the bottom of each panel.

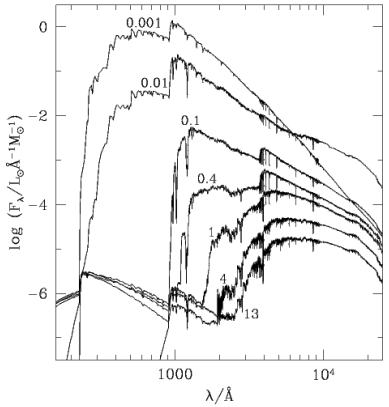

Figure 9. Spectral evolution of the standard SSP model of Section 3 for the solar metallicity. The STELIB/BaSeL 3.1 spectra have been extended blueward of 3200 Å and redward of 9500 Å using the Pickles medium-resolution library. Ages are indicated next to the spectra (in Gyr).

Ages and metallicity are fairly degenerate. One can make a galaxy younger, or make the metallicity lower - and both have roughly the same effect on the spectrum that comes out. This is shown below. Notice that some subtle differences can remain.

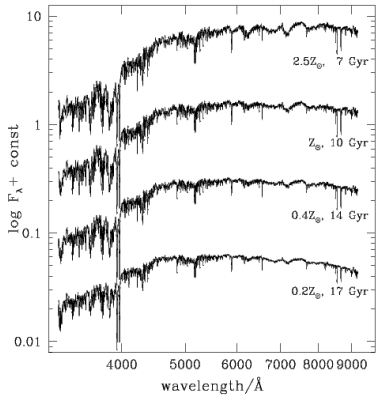

Figure 10. Spectra of the standard SSP model of Section 3 at different ages for different metallicities, as indicated. The prominent metallic features show a clear strengthening from the most metal-poor to the most metal-rich models, even though the shape of the spectral continuum is roughly similar in all models.

Below we analyze how the mass-to-light ratio evolves with time. This is important, as it is used to derive stellar masses from the luminosities. First, we have to realize that much of the light of galaxies comes from the red giant branch. The luminosity of the galaxy is therefore proportional to the number of stars on the RGB, times their average luminosity:

$$L_{tot} \approx L_{GB} * N_{GB}$$

where L_{tot} is total luminosity, L_{GB} is characteristic luminosity of star on the Giant Branch, and N_{GB} is number of stars on the Giant Branch.
We assume a general IMF

$$\frac{dN}{dM} = cM^{-(1+x)}$$

where $x = 1.35$ for a Salpeter mass function.

How many stars are on the RGB ? Calculate the number of stars which turned off from the main sequence between $t = t_0$ and $t = t_0 + T_{RGB}$, where T_{RGB} is the time a star spends on the RGB.
The life time on the main sequence is

$$\frac{t_{MS}}{10Gyr} = \left(\frac{M}{M_\odot}\right)^{-2.5}$$

The higher the mass, the lower the main sequence life time. Hence the turnoff mass is related to age by

$$M_{turnoff} \propto t^{-0.4}$$

The change in the turnoff mass in a time interval $t, t + T_{RGB}$ is

$$dM_{turnoff} \propto \frac{-0.4}{t^{1.4}} T_{RGB} \propto (M^{2.5})^{1.4} T_{RGB} \propto M^{3.5} T_{RGB}$$

the number of stars in that mass interval $M, M + dM_{turnoff}$ is given by

$$dN = dM_{turnoff} * \mathrm{IMF}(M) \propto M^{3.5} M^{-(1+x)}$$

$$\propto M^{(-x+2.5)} \propto t^{0.4x-1}$$

Hence to first approximation, the luminosity of the galaxy evolves like

$$L \propto \frac{1}{t^{1-0.4x}} \quad \text{for } x = 1.35 \quad L \propto \frac{1}{t^{0.46}}$$

Hence the luminosity goes like a power law, and depends on the slope of the IMF around the turn-off mass. In detail, the powerlaw coefficient also depends on the pass band. Young galaxies tend to be bluer than old galaxies in all passbands:

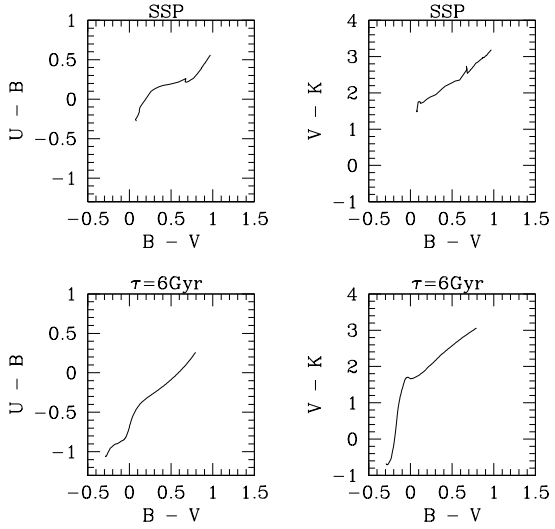

The color-color relations for population models. The colors are shown for ages between 10^8 and 10^{10} years. The colors get redder with time, for all colors

Hence the mass-to-light ratio evolution must be color dependent. Below we normalized the mass-to-light ratios at 2Gyr, to show the dependence on passband, for 1700Å, V-band and K-band

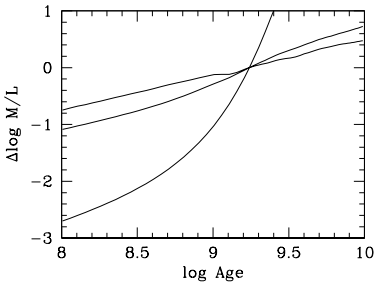

Notice the huge difference between the far UV, and optical and Near-IR bands. The difference between the V band and K band evolution is fairly small. (You'll find erroneous claims in literature that there is no evolution in the M/L_K with time. You can see here how wrong that it).

The color is also well correlated with the M/L ratio. The plots below here show this. This is often used to derive M/L ratios from colors.

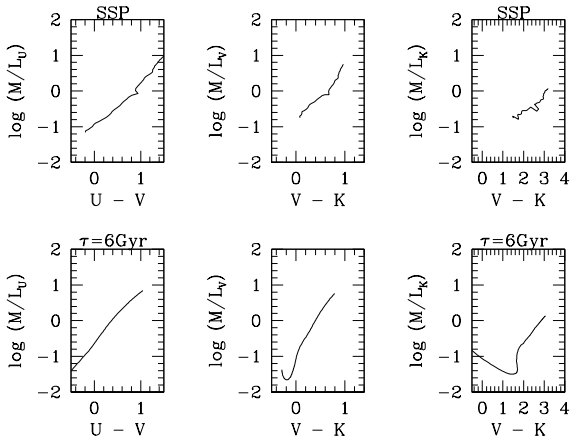

Fig: The colors of a SSP model, for ages between 10^8 and 10^{10} years. Older populations have redder colors, in all passbands shown here.